Analyst

Accepted Manuscript

ROYAL SOCIETY OF CHEMISTRY

www.rsc.org/analyst

Cite this: DOI: 10.1039/c0xx00000x

www.rsc.org/xxxxxx

ARTICLE TYPE

A novel chromo- and fluorogenic dual sensor for Mg^{2+} and Zn^{2+} with cell imaging possibilities and DFT studies†.

Rabiul Alam[a], Tarun Mistri[a], Atul Katarkar[b], Keya Chaudhuri[b] Sushil Kumar Mandal[c], Anisur Rahman Khuda-Bukhsh[c] Kalyan K. Das[a] and Mahammad Ali*,[a]

Received (in XXX, XXX) Xth XXXXXXXXX 20XX, Accepted Xth XXXXXXXXX 20XX

DOI: 10.1039/b000000x

A diformyl-*p*-cresol (DFC)-8-aminoquinoline based dual signaling probe was found to exhibit colormetric and fluorogenic properties on selective binding towards Mg^{2+} and Zn^{2+}. Turn-on fluorescent enhancements (FE) as high as 40 fold and 53 fold in 9:1 MeCN/water (v/v) at pH 7.2 in HEPES buffer for Mg^{2+} and Zn^{2+}, respectively were noticed. The binding constants determined from the fluorescence titration data are: K = (1.52 ± 0.21) x 10^5 M^{-1} and (9.34 ± 4.0) x 10^3 M^{-2} and n =1 and 0.5, for Mg^{2+} and Zn^{2+} respectively. The L:M binding ratios were also determined by Job's method which support the above findings. This is further substantiated by HRMS analysis. Due to solubility in mixed organo-aqueous solvents as well as cell permeability it could be used for the *in vitro*/*in vivo* cell imaging of Mg^{2+} and Zn^{2+} ions with no or negligible cytotoxicity. This probe could be made selective towards Mg^{2+} over Zn^{2+} in presence of TPEN, both in intra- and exctracellular conditions and superior to other Mg^{2+} probes which suffer from selectivity of Mg^{2+} over Ca^{2+} or Zn^{2+}. Not only that the dissociation constant (K_d = 6.60 μM) of Mg^{2+}-(**DFC-8-AQ**) complex is far lower than the so far reported Mg^{2+} probes which fall in the mM range.

Introduction

Mg^{2+} is the most abundant divalent cation in biological systems and considered as an important endogenous protective factor participating in many cellular functions such as enzyme-driven biochemical reactions, proliferation of cells, and stabilization of DNA conformation and regulation of Ca^{2+} signaling.[1]Moreover, Mg^{2+} is also believed to be an etiological factor in many pathological processes, such as congestive heart failure, cerebral infarction, lung cancer, and muscle dysfunction.[2] Magnesium is a cofactor in the phosphorylation of glucose during carbohydrate metabolism[3] and is also required for the proper functioning of nerves and immune systems and for muscle and bone health.[4] It's concentrations in cells typically varies between 0.1 mM and 6 mM: ~0.3 mM in synaptosomes; 0.37 mM in hepatocytes; 0.5 -1.2 mM in cardiac cells, while ~0.44–1.5 mM in normal serum.[5] In diseased states, or under the administration of certain hormonal stimuli or cAMP signaling agents remarkable alterations in [Mg^{2+}] are observed.[6-8] Thus, Mg^{2+} represents an interesting paradox in the human body. While a trace amount is required for normal physiological functions, an unregulated amount may cause serious problems[9] leading to hypermagnesia.[9,10] Hence, measuring Mg^{2+} in the blood serum is a necessary component of epidemiologic studies,[11] and estimation of this mineral in food stuffs may help to formulate guidelines for determining the dietary requirements of diabetic patients. Consequently, the detection of Mg^{2+} has attracted increasing *interest* in the areas of chemical and biological sciences. Although, many analytical methods like atomic absorption, ion-selective electrodes, and NMR[12-14] are available for the detection of Mg^{2+}, optical detection following the changes in fluorescence or absorbance arising from the Mg^{2+} induced perturbation of the chromophore is best suitable for Mg^{2+} detection in biological systems. Thus, to understand the role of Mg^{2+} in various cellular functions development of a simple, selective, and sensitive method for the determination of intracellular Mg^{2+} concentration is very essential. On the other hand, Zn is also very essential for normal cellular functions leading to normal human growth and development. However, a little is known about its intracellular distribution, accumulation and mobility.[15] The major challenge is to apply a Zn-sensor to real-life situation where the intracellular Zn^{2+} concentration

[a] *Department of Chemistry Jadavpur University, Kolkata 700 032, India; Fax: 91-33-2414-6223, E-mail: mali@chemistry.jdvu.ac.in*

[b]Molecular & Human Genetics Division , CSIR-Indian Institute of Chemical Biology , 4 Raja S.C. Mullick Road, Kolkata-700032, India

[c]Department of Zoology, Kalyani University, Kalyani, 741235, India

†Electronic Supplementary Information (ESI) available: See DOI: 10.1039/b000000x/of

spans only in nM range.[16]

The charged β-diketone binding site has been found to have very high selectivity towards Mg^{2+}[17] and a number of such Mg^{2+} selective fluorescent probes are reported in recent years.[18-20] However, most of them and some commercially available Mg^{2+} indicators suffer from the lack of selectivity over Ca^{2+} [21] and also with very high K_d values that essentially lie in few mM range with FE as high as 50 fold.[18-22] So it will be highly desirable to develop a Mg^{2+} probe which can display high selectivity, extensive FE upon complexation and feasibility to apply for intracellular monitoring of Mg^{2+}. Towards this end we have been successful to design a 2,6-diformyl-*p*-cresol(**DFC, 1**)−8-amino-quinoline(**8-AQ, 2**) based sensor (**DFC-8-AQ**), very close to charged β-diketone binding sites that is suitable for preferential sensing of Mg^{2+} in presence of other biologically relevant metal ions and suitable for *in vivo /in vitro* monitoring of Mg^{2+} ion.

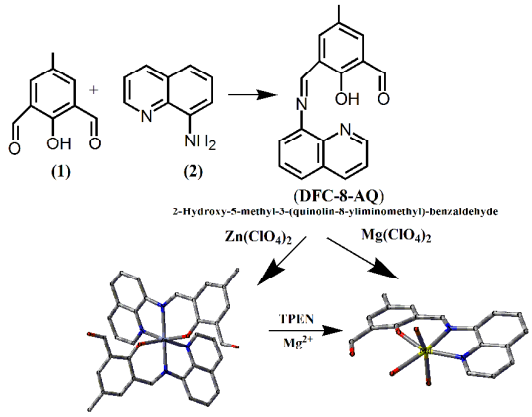

Scheme 1

Results and Discussion

Synthesis of probe (DFC-8-AQ)

The ligand **DFC-8-AQ**, a potential N_2O_2 donor, was prepared by stirring a mixture of 2,6-Diformyl-*p*-cresol (DFC) and 8-amino quinoline in 1:1 mole ratio in ethanol for 5h at room temperature (**Scheme 1**). It was characterized by elemental analyses as well as by various spectroscopic methods like NMR (Figure **S1**) HRMS (Figure **S2**) (Experimental section) etc. The complex **1** (Zn^{2+}-complex) and **2** (Mg^{2+}-complex) were prepared by stoichiometric reaction of $Zn(ClO_4)_2.6H_2O$ and $Mg(ClO_4)_2.6H_2O$ with **DFC-8-AQ** in MeCN and characterized by CHN and Mass analyses (Figures **S2b-S2a**). The microanalyses are in well agreement with the chemical formula's of the complexes (Experimental section). Several trials to grow X-ray quality single crystals of the complexes were not successful.

UV-Vis Absorption Studies

The UV-Vis spectrum of sensor **DFC-8-AQ** was recorded in a CH_3CN-H_2O (9:1 v/v) at pH 7.2, 1.0 mM HEPES buffer (this is the medium for all measurement unless otherwise mentioned) which displayed well-defined bands at 500 and 369 nm. The cation binding affinities of **DFC-8-AQ** toward Mg^{2+} and Zn^{2+} were investigated by UV-Vis spectroscopy. Upon gradual addition of Zn^{2+} to a solution of **DFC-8-AQ** in CH_3CN-H_2O displayed an increase in absorption at 456 nm while bands at 369 and 513 nm gradually decrease generating three isosbestic points at 326, 405 and 500 nm indicating a clean transformation of free ligand to its metal bound state (**Figure 1**). Similar trend was observed with Mg^{2+} but here two isosbestic points at 480 and 411 nm were obtained (**Figure 2**). However, no such significant change in **DFC-8-AQ** spectrum was observed with other tested metal cations. The preferential binding of Mg^{2+} and Zn^{2+} (**Scheme 1**) in the pseudo-cavity of the sensor **DFC-8-AQ** reveals that the sensor binding sites are absorption band complementary to these cations.

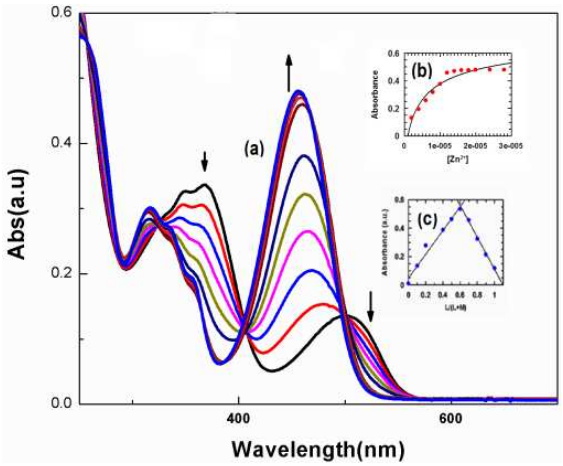

Figure 1. (a) Absorption titration of **DFC-8-AQ** (20 μM) with gradual addition of Zn^{2+}, 2–20 μM in 9:1 v/v MeCN/water in HEPES buffer at pH 7.2. (b) (b) OD_{453} vs. $[Zn^{2+}]$; (c) Job's Plot.

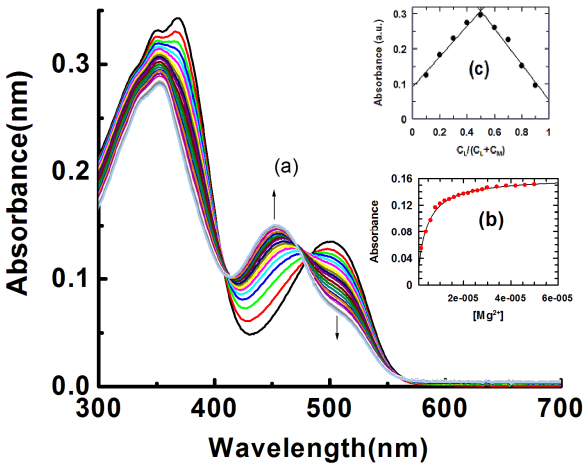

Figure 2.(a) Absorption titration of **DFC-8-AQ** (20μM) in 9:1 v/v MeCN/water in HEPES buffer at pH 7.2 with Mg^{2+}. Inset shows (b) OD_{455} vs. $[Mg^{2+}]$; (c) Job's Plot.

Fluorescence studies

The emission spectra of **DFC-8-AQ** and its fluorescence titration with Zn^{2+} and Mg^{2+} were recorded in CH_3CN-H_2O (**Figures 3 and 4**). The reaction of a metal ion M^{2+} (M = Mg and Zn) with a chelating agent **DFC-8-AQ** induces rigidity in the resulting molecule and tends to produce a large **CHEF** effect which induces the large enhancement of fluorescence. [23] In addition, there is a gradual blue shift of λ_{em} from 562 nm for pure ligand to 539 nm on complexation with Zn^{2+} and to 526 nm with Mg^{2+}. [24] When we plot absorbance or fluorescence intensity as a function of $[M^{2+}]$ non-linear curves were obtained and can be easily solved by using eqn (1), [25] where *a* and *b* are the absorbances/fluoresnces in the absence and presence of excess metal ions, respectively, *c* (= K) is the formation constant and *n* is the stoichiometry of the reactions.

$$y = \frac{a + b*c*x^n}{1 + c*x^n} \qquad (1)$$

The non-linear least-squares curve-fit of the absorption titration data gives: $c = K = (5.25 \pm 2.02) \times 10^3\ M^{-2}$, $n = 0.70$ and $K = (2.00 \pm 0.66) \times 10^5\ M^{-1}$, $n = 1$ for Zn^{2+} and Mg^{2+}, respectively. The corresponding fluorescence titration data to equation (1) gives the parameters: $c = K = (9.34 \pm 4.0) \times 10^3\ M^{-2}$, n =0.50 and $K = (1.52 \pm 0.21) \times 10^5\ M^{-1}$, $n = 1$ for Zn^{2+} and Mg^{2+} respectively. There are reasonable agreements between the data extracted from the two different experiments, namely absorption and fluorescence titrations. The mass spectrum of $[M(\textbf{DFC-8-AQ})]^+$ in MeCN revealed a **DFC-8-AQ**:Mg^{2+} = 1:1 with a peak at m/z = 354.03 ($[Mg(\textbf{DFC-8-AQ})(MeCN)]^+$) while for Zn^{2+} a prominent peak at 650.14 ($[Zn(\textbf{DFC-8-AQ})_2+Li^+]$ indicates a 2:1 complexation with respect to ligand (**Figure S2a-S2b**).

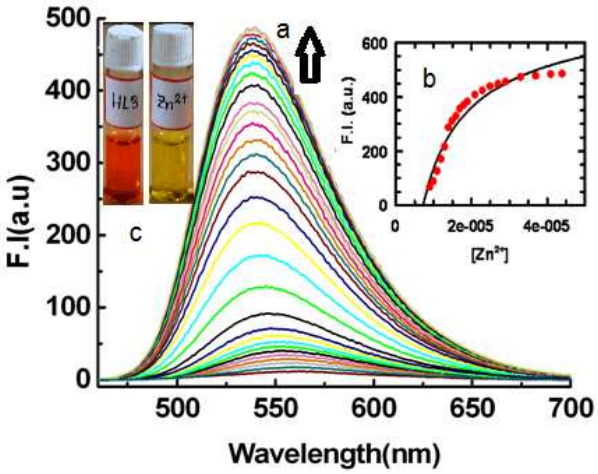

Figure 3. (a) Fluorescence titration of **DFC-8-AQ** (20 µM) in 9:1 v/v MeCN/water in HEPES buffer at pH 7.2 by the gradual addition Zn^{2+} (0-40 µM) with λ_{ex} = 430 nm, λ_{em} = 539 nm Inset (b)Plot of F.I vs. $[Zn^{2+}]$; (c) Naked-eye image of **DFC-8-AQ** and with Zn^{2+}.

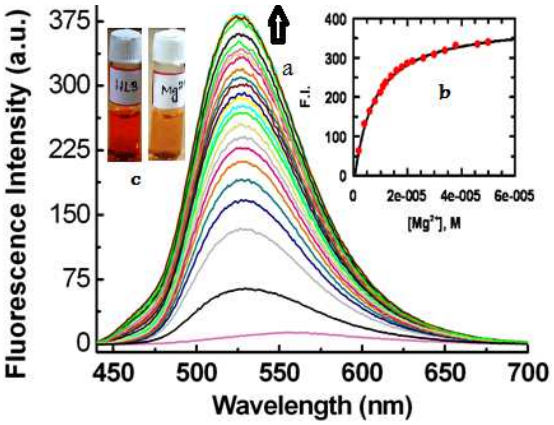

Figure 4. (a) Fluorescence titration of **DFC-8-AQ** (20 µM) in 9:1 (v/v) MeCN/water in HEPES buffer at pH 7.2 by the gradual addition Mg^{2+}(0-50 µM) with λ_{ex} = 430 nm, λ_{em} = 526 nm Inset (b) Plot of F.I vs. $[Mg^{2+}]$; (c) Naked-eye image of **DFC-8-AQ** and with Mg^{2+}.

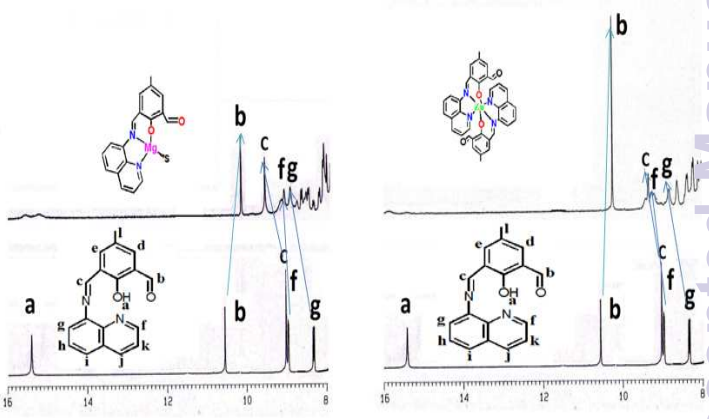

Figure 5. ^{1}H-NMR shifts of free ligand and with addition of 1.5 equivalent of Zn^{2+} and Mg^{2+} in CD_3CN recorded on a 300 MHz Bruker NMR spectrometer.

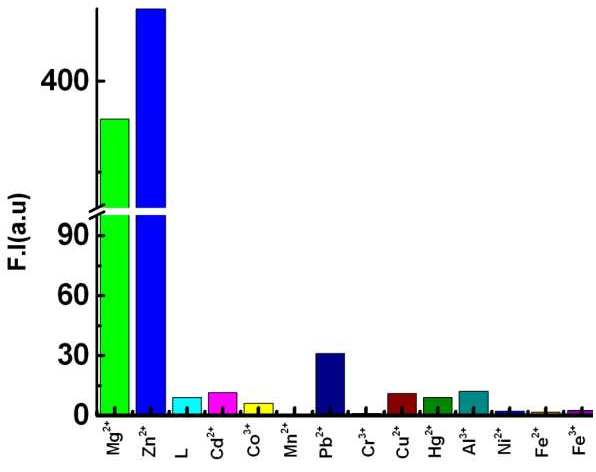

Figure 6. Histogram of the fluorescence responses of different ions (100 µM) towards **DFC-8-AQ** (20 µM) in 9:1 v/v MeCN/water in HEPES buffer at pH 7.2.

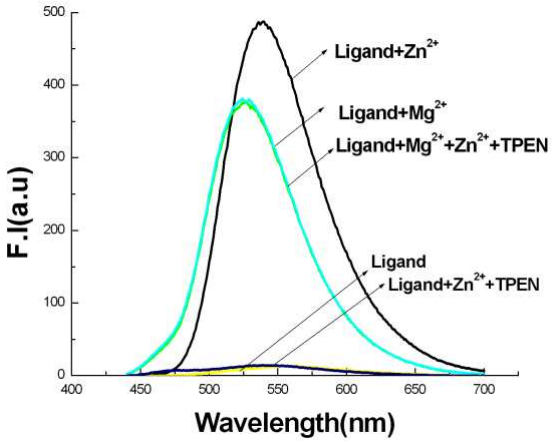

Figure 7. Reversibility plot of Zn^{2+} and Mg^{2+}-complexes in presence of TPEN.

The coordination modes were further supported by ^{1}H-NMR studies (**Figure 5**) which clearly showed a change in chemical shifts of azomethine proton as well as the protons on quinoline moiety (**Table S1**). In the ligand there is an intramolecular H-bonding between formyl oxygen and the –OH group [O-H•••O(formyl) = 1.61 Å , vide infra] resulting a downfield shift of –OH proton as a broad signal to 15.39 ppm. An up-field shift of formyl hydrogen (**b**) signal from 10.53 to 10.16 ppm suggests the removal of H-bonding of formyl O atom with the OH proton of free ligand and its non-participation in bonding to M^{2+} in the complexes. The down-field shift of azomethyne proton(**c**) signal from 9.003 to 9.26 in complex **1** and 9.57 in complex **2** clearly indicates the participation of azomethyne N atom in bonding with the metal ions in both the complexes**.** The proton **g** and **f** are shifted downfield due to coordination of azomethyne and quinoline N atoms to the metal center.

Mg^{2+} and Zn^{2+} detections were not perturbed by biologically abundant Na^{+}, K^{+}, Ca^{2+} etc metal ions **(Figure S3)**. Several transition metal ions, namely Cr^{3+}, Mn^{2+}, Fe^{2+}, Fe^{3+}, Co^{2+}, Ni^{2+}, Cu^{2+}, and heavy metal ions like Cd^{2+}, Pb^{2+}, and Hg^{2+}, also caused no interference (**Figure 6**). The sensor was found to bind M^{2+} reversibly as tested by reacting with EDTA. (**Figure S4**). However, in presence of TPEN the fluorescence is completely masked for Zn^{2+} but for Mg^{2+} this remains almost unchanged favouring the selective detection of Mg^{2+} in presence of Zn^{2+} (**Figure 7**), which is the added advantage of this probe over other reported or commercially available Mg^{2+} probes that recognise other metal ions like Ca^{2+} or Zn^{2+} along with Mg^{2+}. Not only that the dissociation constant (K_d = 6.60 μM) of Mg^{2+}-(**DFC-8-AQ**) complex is far lower than the so far reported Mg^{2+} probes which falls in the mM range. Quantum yields of the **DFC-8-AQ**, and its Zn^{2+} and Mg^{2+} complexes were determined with values Zn (0.163) and Mg (0.131) which are 3-4 times higher than the pure **DFC-8-AQ** (0.043). LOD for Mg2+ and Zn2+ were determined by 3σ method which are found to be 2.04 and 5.81 nM respectively (Fig **S9** in SUP data)

We have also recorded the absorption and fluorescence spectra of the free ligand (20 μM), its Mg^{2+}(20 μM L + 30 μM Mg^{2+}) and Zn^{2+} +(20 μM L + 30 μM Zn^{2+}) complexes in 9:1, 8:2, 7:3, 6:4, 1:1, 4:6, 3:7, 2:8 and 1:9, v/v, MeCN-H_2O solvent mixtures. Though there is a very slight increase in absorbance as well as fluorescence intensity of the free ligand with the increase in water content, there no visible change in them in case of Zn^{2+} complex, whereas in case of Mg^{2+} complex there is a decrease in absorbance as well as FI with the increase in water content (Please See the **Figure S5** in the Supporting Information).

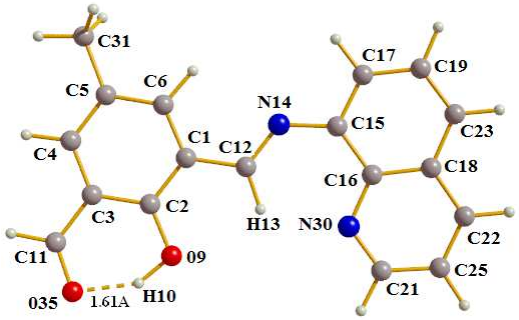

DFC-8-AQ

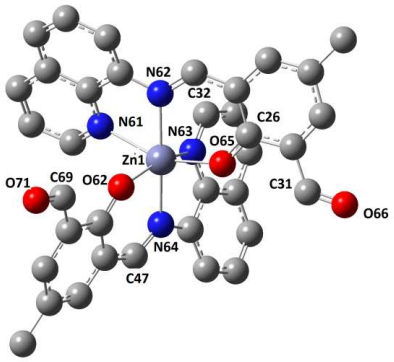

[Zn(DFC-8-AQ)$_2$] (1)

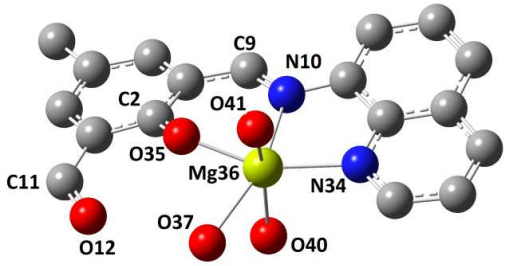

[Mg(DFC-8-AQ)(H$_2$O)$_3$] (2)

Figure 8. Optimized geometries of DFC-8-AQ, $[Mg(DFC\text{-}8\text{-}AQ)(H_2O)_3]^+$ and $[Zn(DFC\text{-}8\text{-}AQ)_2]$

Geometry optimization and electronic structure

Geometries of **DFC-8-AQ** and complexes, **[Zn(DFC-8-AQ)$_2$](1)** and **[Mg(DFC-8-AQ)(H$_2$O)$_3$]$^+$(2)** were fully optimized using B3LYP functional as implemented in Gaussian 03.[26] The nature of all the stationary points was confirmed by carrying out a normal

mode analysis, where all vibrational frequencies were found to be positive. Some selected optimized geometrical parameters of **DFC-8-AQ** and complexes **1** and **2** are listed in Table 1 and geometry optimized structures are given in Figure 8.

The modelled geometry of complex **1** and **2** possess a distorted octahedral arrangement around the central metal ions. In **1** all the calculated Zn-N/Zn-O distances fall in the range 2.054 - 2.319 Å and comparable to the reported values in the analogous complexes.[27] The two formyl groups present in the two coordinated ligands remain uncoordinated and this is in conformity of ^{1}H NMR studies which showed up-field shift of formyl hydrogen (**b**) signal from 10.53 to 10.16 ppm (Figure 5). In case of complex **2**, one **DFC-8-AQ** with N_2O donor atoms and three water molecules surround the Mg atom giving it a distorted octahedral geometry. Here also the formyl group remained uncoordinated and supported by ^{1}H NMR studies. On complexation some C-N and C-O bond lengths are slightly changed with respect to those in free ligand (Table 1).

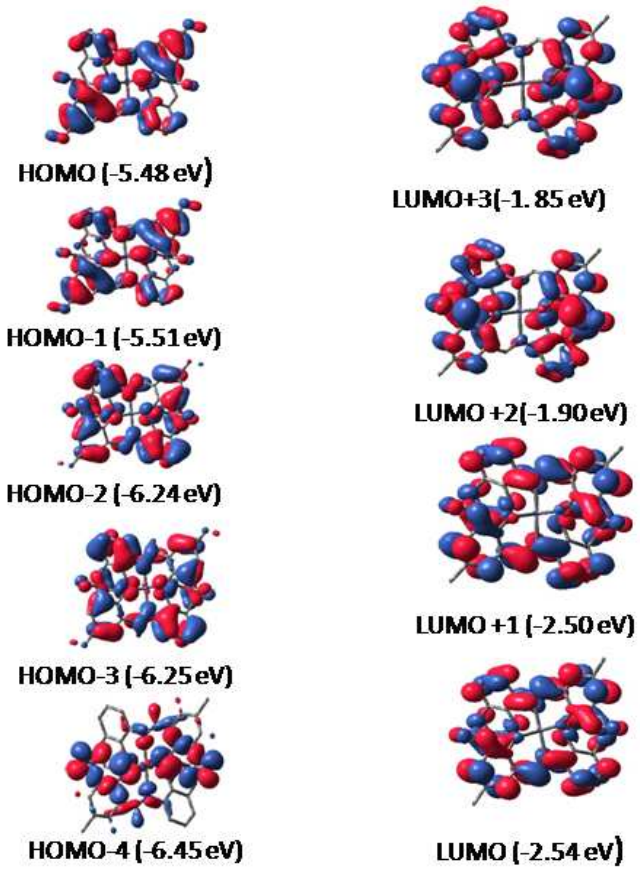

Figure 9. MO diagrams for the [Zn(**DFC-8-AQ**)$_2$]

Table 1 Selected optimized geometrical parameters for DFC-8-AQ and complexes **1** and **2** in the ground state calculated at B3LYP Levels.

Bond Distance (Å)		Bond Distance (Å)	
C1-C12	1.46	N14-C12	1.29
N30-C21	1.32	C2-O9	1.35
N30-C16	1.36	C11-O35	1.26

Bond Distance (Å)		Bond Angles (°)	
Zn1-N61	2.318	N61 -Zn1-N63	87.00
Zn1-N62	2.195	N61 -Zn1-O67	87.60
Zn1-N63	2.319	N63 -Zn1-O65	87.70
Zn1-N64	2.195	O65 -Zn1-O67	105.7
Zn1-O65	2.054	N61 -Zn1-O67	176.4
Zn1-O67	2.054	N62 -Zn1-N64	73.60
C69-O71	1.227	N61 -Zn1-N64	103.8
C31-O66	1.227	N61 -Zn1-N64	96.50
C56-O67	1.280	N64 -Zn1-O67	85.70
C26-O65	1.280		

Bond Distance (Å)		Bond Angles (°)	
Mg36-N10	2.179	N10-Mg36-N34	77.1
Mg36-N34	2.176	O35-Mg36-N10	83.9
Mg36-O35	1.960	O35-Mg36-O37	77.4
Mg36- O37	2.214	O34-Mg36-O37	124.2
Mg36- O41	2.145	O37-Mg36-O40	74.6
Mg36- O40	2.50	O40-Mg36-O41	158.6
C2-O35	1.254	N10-Mg36-O41	106.8
C11-O12	1.233	N34-Mg36-O41	90.16
		N10-Mg36-O40	94.2
		N34-Mg36-O40	90.8

Time dependent density functional theory (TDDFT)[28-30] with B3LYP density functional was applied to study the low-lying excited states of the complex in MeCN using the optimized geometry of the ground (S_0) state. The vertical excitation energies of the lowest 20 singlet states are also computed here.

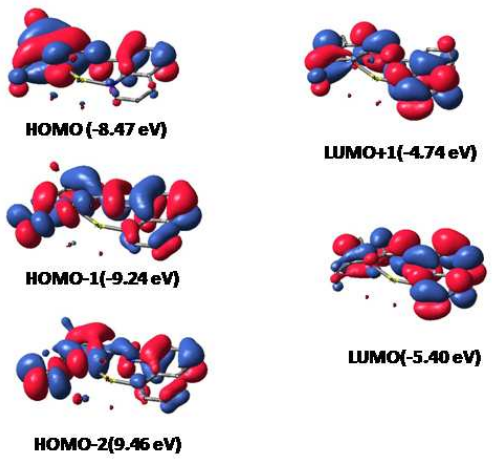

Figure 10. MO diagrams for the $[Mg(\textbf{DFC-8-AQ})(H_2O)_3]^+$

The UV spectra computed from TDDFT calculations in MeCN show two important peaks in the range 300-600 nm (See **Figures S5-S6**). For complex **1**, the band around 455 nm is dominated by the HOMO→LUMO+1 and HOMO-1 → LUMO+1 excitations, while the band around 347 nm is mainly due to HOMO-3→LUMO+1 and HOMO-4 →LUMO transitions. The details of the vertical excitation energies, oscillator strengths, and nature of excitations are shown in **Table 2**. For complex **2** the band around 447 nm is dominated by the HOMO→LUMO excitation, while the band around 343 nm is mainly due to HOMO-2→LUMO transitions as depicted in **Table 2**. Here, calculated spectra of the complexes are found to be in excellent match with the experimental ones with λ_{max} (absorption) values calculated (experimental): 455 (456) and 347 (368) nm for Zn^{2+} and 447 (453) and 343 (369) nm for Mg^{2+} (Figure **S6-S8**)**.** MO diagrams of Zn^{2+} and Mg^{2+} complexes are shown in **Figure 9** and **10** respectively.

Table 2. Vertical excitation energies (E_{cal}), oscillator strengths (f_{cal}), and type of excitations of the lowest few excited singlets obtained from TDDFT calculations of **$[Zn(DFC\text{-}8\text{-}AQ)_2]$** and **$[Mg(DFC\text{-}8\text{-}AQ)(H_2O)_3]^+$** in MeCN.

compound	State	E_{cal}/n	f_{cal}	excitation
$[Zn(DFC\text{-}8\text{-}AQ)_2]$ (**1**)	S_1	459	0.2535	HOMO-1→LUMO (0.34), HOMO→LUMO+1 (0.34),
	S_2	455	0.3777	HOMO→LUMO+1 (0.68) HOMO−1→LUMO+1 (0.68),
	S_4	448	0.2897	HOMO→LUMO+1 (0.68)
	S_{14}	347	0.2175	HOMO−3→LUMO+1 (0.48), HOMO−4→LUMO (0.26), HOMO−2→LUMO (0.24), HOMO−5→LUMO+1 (0.15) HOMO−5→LUMO+2 (0.13) HOMO−4→LUMO+3 (0.12)
$[Mg(DFC\text{-}8\text{-}AQ)(H_2O)_3]^+$ (**2**)	S_1	447	0.4944	HOMO→LUMO (0.87),
	S_4	343	0.1231	HOMO−2→LUMO (0.24)

***p*H studies**

The dependences of fluorescence intensity of the free ligand and its Mg^{2+} and Zn^{2+} complexes on the pH of the medium were investigated in the range pH 2.0 to 10.0 at **[DFC-8-AQ]** = 20 μM, $[M^{2+}]$ 30 μM in 9:1 MeCN:H_2O v/v in HEPES buffer(**Figure 11**). It was observed that in the above mentioned *p*H range the FI of the free ligand remains almost constant at ~ 9.0 ± 1.0. However, on addition of 1.2 equivalents of Mg^{2+} the FI jumps to 350 ± 20 and remains constant in the range pH 2-8, but on further increase in pH the FI gradually falls. Similar is the trend in case for Zn^{2+} complex but here FI remains almost constant at ~ 500 ± 20 in the range pH 2-8 and then drastically falls to FI ~115 due to the removal of Zn^{2+} from the complex with the formation of $Zn(OH)_2$ at pH> 8.0. The slightly higher value of FI of the complexes than that of free ligand may be due to the fact that certain fraction the complex remains undissociated in solution phase at pH ~10.0.

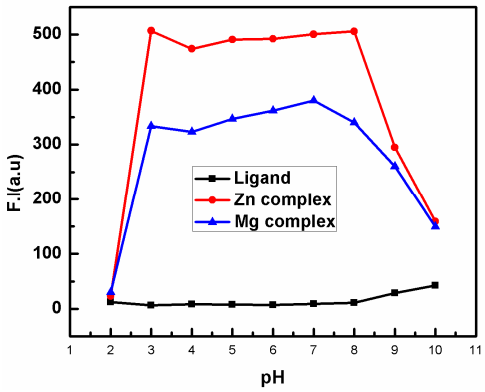

Figure 11. pH dependence of fluorescence responses of DFC-8-AQ and its Zn^{2+} and Mg^{2+}-complexes in 9:1 (v/v) MeCN/water.

Cell Imaging and Cytotoxicity Studies

To test the cytotoxicity of **DFC-8-AQ** in HepG2 cells, 3-(4, 5-dimethyl-thiazol-2-yl)-2,S-diphenyltetrazolium bromide (MTT) assay was performed as per the procedure described earlier[31] which revealed that after treatment with **DFC-8-AQ** at different doses of 1, 10, 20, 50 and 100 μM, respectively for 12 h no significant cytotoxicity was observed.(**Figure 12**)

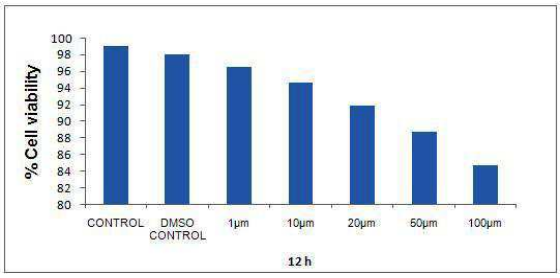

Figure 12. Represents % cell viability of HepG2 cells treated with different concentrations (1 μM-100 μM) of **DFC-8-AQ** for 12 hrs determined by MTT assay. Results are expressed as mean of three independent experiments.

The intracellular Mg^{2+} imaging behaviours of **DFC-8-AQ** on HepG2 cells with the aid of fluorescence microscopy displayed intracellular fluorescence when treated with 10µM **DFC-8-AQ** (**Figure 13**)**.** The same intensity was observed after external addition of *tetrakis*-(2-Pyridylmethyl)ethylenediamine (TPEN) 100 µM. However, cells exhibited intense fluorescence behaviour when the **DFC-8-AQ** pre-incubated cells were added externally with Mg^{2+} and Zn^{2+} (10 µM each) separately. The fluorescence behaviour of the cells pre-exposed to Zn^{2+} ion (10 µM) was, however, suppressed when incubated with TEPN (100 µM) because of a strong scavenging action of TPEN on Zn^{2+} ions (**Figure 13**). Again, when cells pre-exposed with both the metal ions were treated with TPEN (100 µM), there was an intense fluorescence, as it did not block the Mg^{2+} ions (**Figure 13**). Therefore, this renders confirmatory evidence of the sensor having the ability to perform a dual roles, both as a sensor of Mg^{2+} and Zn^{2+} ions, and either singly or in combination; and may find application in biological monitoring of these metal ions, because of its relatively low cytoxicity up to 12 hr (**Figure 12**), at the indicated dose and time of incubation.

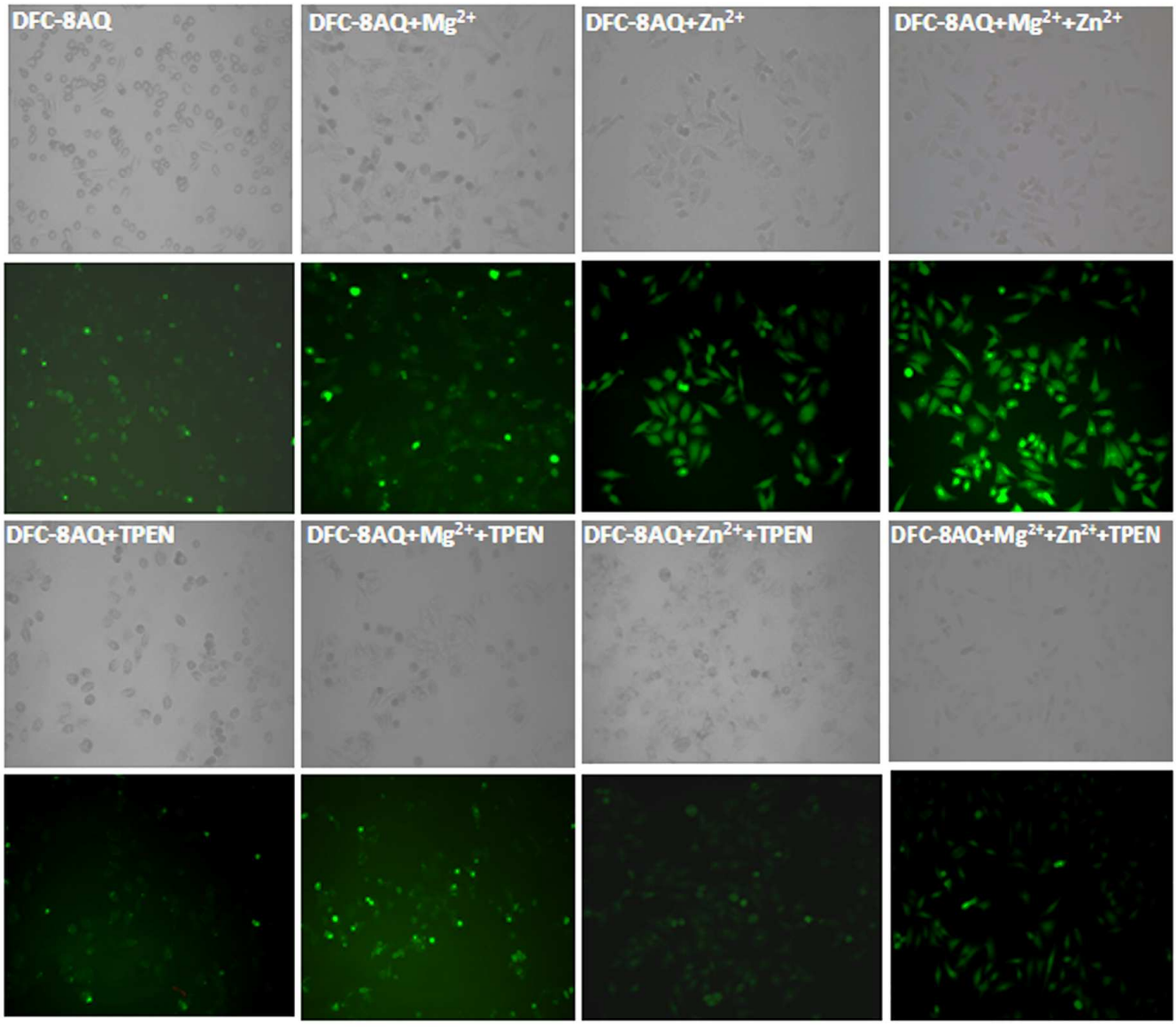

Figure 13. The phase contrast and fluorescence images of HepG2 cells were capture after being incubated with **DFC-8-AQ, DFC-8-AQ+** $Mg^{2+,}$ **DFC-8-AQ+** Zn^{2+} and **DFC-8-AQ+** Mg^{2+}+Zn^{2+} for 30 min at 37 °C and followed by addition of 100 µM TPEN after 30 min pre-incubated with **DFC-8-AQ, DFC-8-AQ+** $Mg^{2+,}$ **DFC-8-AQ+** Zn^{2+} and **DFC-8-AQ+** Mg^{2+}+Zn^{2+} and allow incubation for next 30 min.

Cite this: DOI: 10.1039/c0xx00000x

www.rsc.org/xxxxxx

ARTICLE TYPE

In summary, we have been successful to design and synthesize a novel **DFC-8-AQ** based highly selective Mg^{2+} sensor which displayed 40 fold in 9:1 MeCN:H_2O v/v at pH 7.20 in 1 mM HEPES buffer) as well as the highest formation constant (K) value with the possibility of *in vivo* dynamic monitoring of Mg^{2+} concentration. Not only that, whereas most of the previously reported probes suffer from selectivity of Mg^{2+} over Ca^{2+}, that is present in high concentration in cellular system, this probe is highly selective towards Mg^{2+} and Zn^{2+}, which can further be selective towards Mg^{2+} when Zn^{2+} is masked by TPEN.

Materials and Methods

The starting materials such as 8-aminoquinoline (Sigma Aldrich), 2,6-Diformyl-*p*-cresol (DFC) prepared in the laboratory) were used for the preparation of ligands **DFC-8-AQ.** $Mg(ClO_4)_2.6H_2O$ (Merck, Germany), and $Zn(ClO_4)_2.6H_2O$ was used to prepare Mg^{2+}-complex and Zn^{2+}-complex, respectively. Solvents like MeCN, Ethanol, (Merck, India) were of reagent grade and dried before use.

Preparation of 2-Hydroxy-5-methyl-3-(quinolin-8-yliminomethyl)-benzaldehyde (DFC-8-AQ): 2,6-Diformyl-*p*-cresol (DFC) was prepared by following a literature procedure.[23b] 2,6-Diformyl-*p*-cresol (DFC) (1.64 g, 10 mmol) was dissolved in 25 mL EtOH under nitrogen atmosphere. To this solution was added 8-amino quinoline (1.44 g, 10 mmol) and stirred at room temperature for 5h and then the reaction mixture was filtered out and kept at room temperature. After 1 day crystalline product was deposited. (yield, 80%). Anal. Calcd for $C_{18}H_{14}N_2O_2$: C,74.47; H, 4.86; N, 9.65. Found: C, 74.57; H, 4.87; N, 9.69. ^{1}H-NMR (in CD_3CN) (δ, ppm): 2.35 (s, 3H), 7.57-7.61(m, 1H), 7.64-7.66(m, 1H) ,7.70-7.73 (m,3H), 7.85(d, *J* = 7Hz,1H), 8.31(d, *J*=6.8Hz, 1H), 8.94(dd, *J* = 7.2,4.2 Hz, 1H), 9.0 (s, 1H); 10.53 (s, 1H); 15.4 (s, 1H) (please see **Figure S1** for ^{1}H-NMR). ESI-MS^+ (m/z): 291.05 (L+H^+) [**Figure S2**]. ^{13}C NMR (dmso-d_6, 300 MHz): δ 19.69, 117.72, 120.05, 122.40, 123.24, 124.38, 126.24, 128.67, 133.09, 136.34, 137.32, 139.91, 141.51, 146.93, 150.84, 162.32, 165.74, 189.00[**Figure S1(a)**].

Preparation of Complex 1 and 2

Complex 1. $Zn(ClO_4)_2.6H_2O$ (0.186 g 0.5 mmol) was dissolved in 10 ml of MeCN and to this solution, the ligand **DFC-8-AQ** (0.290 g, 1 mmol) was added. The color of the solution changed to bright yellow. The resulting mixture was stirred for 3 h. The volume of the solution was then reduced to 5 ml under reduced pressure and diethyl ether (10 ml) was added and kept at 0 °C for 12 h to afford complex **1** as microcrystals. Yield: .398g (~70%). CHN analyses for ([Zn(**DFC-8-AQ**)$_2$]) $C_{36}H_{26}N_4O_4Zn$ (M.W.644), Calcd (%): C, 67.14; H 4.07;N, 8.70. Found (%): C, 67.16, H 4.10, N 8.81. UV-vis.(MeCN): λ_{max}, 453 nm (**Figure 1**).

Complex 2. $Mg(ClO_4)_2.6H_2O$ (0.331 g, 1 mmol) was dissolved in 10 ml of MeCN and to this solution, the ligand **DFC-8-AQ** (0.290 g,1 mmol) was added. The color of the solution changed to yellow. The resulting mixture was stirred for 3 h. The volume of the solution was reduced to 5 ml under reduced pressure and diethyl ether (10 ml) was added and kept at 0 °C for 12 h to afford complex **1** as microcrystals. Yield: .356g (~60%). CHN analyses for ([Mg(**DFC-8-AQ**)(CH_3CN)]) $C_{20}H_{16}N_3O_2Mg$ (M.W.354), Calcd (%): C, 67.73; H 4.55; N, 11.85. Found (%): C, 67.82, H 4.70, N 12.12. UV-vis. (MeCN): λ_{max} 455 nm (**Figure 2)**

Physical Measurements

Elemental analyses were carried out using a Perkin–Elmer 240 elemental analyzer. ^{1}H-NMR was recorded in $CDCl_3$ on a Bruker 300 MHz NMR Spectrometer using tetramethylsilane (δ = 0) as an internal standard. UV-Vis spectra were recorded on an Agilent diode-array spectrophotometer (Model, Agilent 8453), Steady-state Fluorescence spectra were recorded on a Shimadzu spectro-fluorimeter (Model RF-5301.), ESI-MS^+ (m/z) of the ligand and its $Mg^{2+}$and Zn^{2+} complexes were recorded on Waters HRMS spectrometers (Model: QTOF Micro YA263 and Model: XEVO-G2QTOF#YCA351)

Computational details

DFT calculations on **DFC-8-AQ , [Zn(DFC-8-AQ)$_2$]** and **[Mg(DFC-8-AQ)$(H_2O)_3$]$^+$** were fully optimized using Gaussian 03 program.[26] The B3LYP functional has been adopted along with 6-31++G(d,p) basis set for H, C, N, O atoms and LANL2DZ effective core potentials and basis set for the Zn atom. In case of **[Mg(DFC-8-AQ)$(H_2O)_3$]$^+$** 6-31++G(d,p) basis set was used for all the atoms including Mg. The global minima of all these species were confirmed by the positive vibrational frequencies**.** Time dependent density functional theory (TDDFT)[28-30] with B3LYP density functional was applied to study the low-lying excited states of the complex in MeCN using the optimized geometry of the ground (S_0) state. The vertical excitation energies of the lowest 20 singlet states are also computed here. The UV spectra were computed from TDDFT calculations in MeCN.

Cell culture

HepG2 cell line, Human hepatocellular liver carcinoma cells, were procured from National Center for Cell Science, Pune, India, and used throughout the study. Cells were cultured in DMEM (Gibco BRL) supplemented with 10% FBS (Gibco BRL), and a 1% antibiotic mixture containing PSN (Gibco BRL) at 37°C in a humidified incubator with 5% CO_2 and cells were grown to 80-90% confluence, harvested with 0.025% trypsin (Gibco BRL) and 0.52 mM EDTA (Gibco BRL) in phosphate-buffered saline (PBS), plated at the desired cell concentration and allowed to re-equilibrate for 24 h before any treatment.

Cytotoxicity and Cell Imaging Studies

To test the cytotoxicity of **DFC-8-AQ**, 3-(4, 5-dimethyl- thiazol-2-yl)-2,S-diphenyltetrazolium bromide (MTT) assay was performed as per the procedure described earlier.[31] After treatment with DFC-8-AQ at different doses of 1, 10, 20, 50 and 100 µM, respectively, for 12 h, 10 µl of MTT solution was added to each well, and the mixture was incubated for 4 h at 37°C. To achieve solubilisation of formazan crystals formed in viable cells, 100 µl of dimethyl sulfoxide (DMSO) was added to each well and the optical density was measured at 550 nm (OD_{550}) (EMax precision microplate reader; Molecular Devices). The percentage of cytotoxicity was calculated as cytotoxicity = $(1 - A_{test}/A_{control}) \times 100$. Cells were incubated with 10 µM **DFC-8-AQ** [1 mM stock solution was prepared by dissolving **DFC-8-AQ** in DMSO: water = 1:9 (v/v)] in the culture medium for 30 min at 37 °C and then washed twice with phosphate-buffered saline (PBS). After that the bright field and fluorescence images of HepG2 cells were taken by a fluorescence microscope (Leica DM3000, Germany) with an objective lens of 20X magnification; fluorescence images of HepG2 cells incubated with 10 µM **DFC-8-AQ** for 30 min followed by addition of a mixture of both 10 µM Mg^{2+} ions ($Mg(ClO_4)_2$) and 10 µM $Zn(ClO_4)_2$ were taken and similarly two sets of experiments were done, one with the addition of only 10 µM $Mg(ClO_4)_2$ and the other, with the addition of only 10 µM $Zn(ClO_4)_2$ instead of addition of both the metal ions simultaneously, fluorescence images were taken separately. Another experiment was done with the sensor plus Zn^{2+} ions together with 100 µM TPEN and fluorescence images were then taken. Similarly another set of experiments were carried out and fluorescence images of HepG2 cells, after being incubated at 37 °C with 10 µM **DFC-8-AQ** for 30 min followed by 15 min incubation with a mixture of both 10 µM extracellular Mg^{2+} ions and 10 µM extracellular Zn^{2+} ions together with 100µM TPEN were taken.

Acknowledgement

Financial supports from CSIR (Ref. 02(2490)/11/EMR-II) and DST (Ref. SR/S1/IC-20/2012) New Delhi, are gratefully acknowledged.

References

1 (a) H. Rubin, *Arch. Biochem. Biophys*., 2007, **458**, 16; (b) J. A. Cowan, *Biometals.,* 2002, **15**, 225; (c) F. I. Wolf, A. Torsello, A. Fasanella and A. Cittadini, *Mol. Aspects Med*., 2003, **24**, 11; (d) N. E. L. Saris, E. Mervaala, H.Karppanen, J. A.Khawaja and A.Lewenstam, *Clin. Chem. Acta*., 2000, **294**, 1; (e) H. Rubin, *Bioessays.,* 2005, **27**, 311.

2 (a) O. B. Stepura and A. I. Martynow, *Int. J. Cardiol*., 2009, **134**, 145; (b) S. C. Larsson, M. J. Virtanen, M. Mars, S. Männistö, P. Pietinen, D. Albanes and J. Virtamo*, Arch. Intern. Med*., 2008, **168**, 459; (c) S. Mahabir, Q. Y. Wei, S. L. Barrera, Y. Q. Dong, C. J. Etzel, M. R. Spitz and M. R. Forman, *Carcinogenesis*., 2008, **29**, 949.

3 (a) B. O'Rourke, P. H. Backx and E. Marban, *Science.,* 1992, **257**, 245; (b) H. C. Politi and *R. R.* Preston, *Neuroreport.,* 2003, **14**, 659; (c) L.-J. Dai, G. Ritchie, D. Kerstan, H. S. Kang, D. E. C. Cole and G. A. Quamme, *Physiol. Rev*. 2001, **81**, 51; (d) C. Schmitz, A. Perraud, C. O. Johnson,. K. Inabe, M. K. Smith, R. Penner, T. Kurosaki, A. Fleig and A. M. Scharenberg, *Cell* .,2003, **113**, 191;

4 (a) A. Ajayaghosh, E. Arunkumar and J. Daub, *Angew. Chem.,* Int. Ed. 2002, **41**, 1766; (b) H. J. Kim and J. S. Kim*, Tetrahedron Lett*., 2006, **47**, 7051; (c) S. Mahabir, Q. Y. Wei, S. L. Barrera, Y. Q. Dong, C. J. Etzel, M. R. Spitz and M. R. Forman, *Carcinogenesis.,* 2008, **29**, 949; (d) F. H. Nielsen and H. C. Lukaski, *Magnes. Res.*, 2006, **19**, 180; (e) G. Farruggia, S. Lotti, L. Prodi, M. Montalti, N. Zaccheroni, P. B. Savage, V. Trapani, P. Sale and F. Wolf, *J. Am. Chem. Soc*., 2006, **128**, 344.

5 E. Murphy, C. C. Freudenrich and M. Lieberman, *Annu. Rev. Physiol.*, 1991, **53**, 273.

6 D. P. Chaudhary, R. Sharma and D. D. Bansal, *a review. Biol. Trace Elem. Res.,* 2010, **134**, 119.

7 A. Romani, *Arch Biochem. Biophys.,* 2007, **458**, 90.

8 B. Sontia and R. M. Touyz, *Arch Biochem Biophys*., 2007, **458**, 33.

9 G. I. Koldobskii and V. A. Ostrovskii, *Usp. Khim.,* 1994, ***63***, 847.

10 (a) F. Guerrero-Romero and M. Rodriguez-Moran, *Acta Diabetol.,* 2002, **39**, 209; (b) C. Bradford and A. McElduff, *Crit. Care Resusc*., 2006, **8**, 36.

11 W. R Carpenter, *J. Org. Chem.,* 1962, ***27***, 2085-2088.

12 M. D. Yago, M. Manas and J. Singh, *Front. Biosci*., 2000, **5**, D602.

13 A. Romani, C. Marfella and A. Scarpa, *Circ. Res.,* 1993, **72**, 1139.

14 H. J. Kennedy, *Exp. Physiol*., 1998, **83**, 449-460.

15 (a) E. Tomat and S. J. Lippard *Inorg. Chem.* 2010, ***49***, 9113; (b) K. Komatsu, Y. Urano, H. Kojima and T. Nagano, *J. Am. Chem. Soc*., **2007**, 129, 13447; (c) K. R. Gee, Z.-L. Zhou, W.-J. Qian and R. Kennedy *J. Am. Chem. Soc*., **2002**, 124; (d) Y.Li, J. Wu, X. Jin, J. Wang, S. Han, W. Wu, J. Xu, W. Liu, X. Yao and Y. Tang , *Dalton Trans.*, 2014, **43**, 1881.

16 (a) K. R. Gee, Z. L Zhou, D. Ton-That, S. L. Sensi and J. H. Weiss, *Cell Calcium.,* **2002**, *31*, 245; (b) K. R. Gee, Z. L. Zhou, W. J. Qian and R. Kennedy, *J. Am. Chem. Soc.,* 2002, **124**, 776; (c) (c) E. J. Song, J. Kang, G. R. You, G. J. Park, Y. Kim, S.-J. Kim, C. Kim and R. G. Harrison, *Dalton Trans.***,** 2013, **42**, 15514; (d) G. K. Tsikalas, P. Lazarou, E. Klontzas, S. A. Pergantis, I. Spanopoulos, P. N. Trikalitis, G. E. Froudakis and H. E. Katerinopoulos, *RSC Adv.***,** 2014,**4**, 693; (e) ***Dalton Trans.***, 2013,**42**, 16569-16577,Kyung Beom Kim, Hyun Kim, Eun Joo Song, Sumi Kim, Insup Noh and Cheal Kim; (f) P. Li, X. Zhou,

R. Huang, L. Yang, X. Tang, W. Dou, Q. Zhao and W. Liu, *Dalton Trans.*, 2014, **43**, 706; (g) Z. Liu, C. Zhang, Y. Chen, F. Qian, Y. Bai, W. He and Z. Guo, *Chem. Commun.*, 2014,**50**, 1253;

17 H. Komatsu, N. Iwasawa, D. Citterio, Y. Suzuki and T Kubota, *J Am Chem Soc.,* 2004,**126**, 16353.

18 Y. Suzuki, H. Komatsu, T. Ikeda, N. Saito and S. Araki, *Anal. Chem.,* 2002 **74**, 1423.

19 T. Shoda, K. Kikuchi, H. Kojima, Y. Urano and H. Komatsu, *Analyst*., 2003, **128**, 719.

20 H Komatsu, T Miki, D Citterio, T Kubota and Y Shindo, *J Am Chem Soc.,* 2005, **127**, 10798.

21 B. Raju, E. Murphy, L. A. Levy, R. D. Hall and R. E. London, *Am J Physiol.,* 1989, **256**, C540.

22 X. Zhou, B. Yu, Y. Guo, X. Tang, H. Zhang and W. Liu, *Inorg. Chem*., 2010, **49**, 4002.

23 a) P. Ashokkumar, V. T. Ramakrishnan and P. Ramamurthy, *J. Phys. Chem. A.,* 2011, **115**, 14292; (b) T. Mistri, M. Dolai, D. Chakraborty, A. R. Khuda-Bukhsh, K. K. Das and M. Ali, *Org. Biomol. Chem*., 2012,**10**, 2380; (c) T. Mistri, R. Alam, M. Dolai, S K. Mandal, A. R. Khuda-Bukhsh and M. Ali, *Org. Biomol. Chem.*, 2013,**11**, 1563.

24 J. Y Choia, D. Kimb and J. Yoon, *Dyes and pigment s.,* 2013, **96**,176.

25 C. R. Lohani, J.-M. Kim, S.-Y. Chung, J. Yoon and K.-H. Lee, *Analyst,*.2010, **135**, 2079.

26 M. J. Frisch, et al., Gaussian 03, revision C.02; Gaussian, Inc.: Wallingford, CT, 2004.

27 X. Zhou, B. Yu, Y. Guo, X. Tang, H. Zhang and Weisheng Liu, *Inorg. Chem.,* 2010, **49**, 4002.

28 A. D. Becke, *J. Chem. Phys*., 1993, **98**, 5648.

29 P. J. Hay and W. R. Wadt, *J. Chem. Phys*., 1985, **82**, 299.

30 (a) S. Miertus, E. Scrocco and J. Tomasi, *Chem. Phys*., 1981**, 55**,117;(b) V. Barone, M. Cossi and J. Tomasi, *J. Comput. Chem.,* 1998, **19**, 404.

31 T. Mossman, *J. Immunol. Methods.,*65(1983), 55-63.

TOC

A novel chromo- and fluorogenic dual sensor for Mg^{2+} and Zn^{2+} with cell imaging possibilities and DFT studies†.

Rabiul Alam[a], Tarun Mistri[a], Atul Katarkar[b], Keya Chaudhuri[b] Sushil Kumar Mandal[c], Anisur Rahman Khuda-Bukhsh[c] Kalyan K. Das[a] and Mahammad Ali*,[a]

A diformyl-*p*-cresol (DFC)-8-aminoquinoline based signaling probe was found to exhibit dual colormetric and fluorogenic properties on selective binding towards Mg^{2+} and Zn^{2+}. This probe could be made selective towards Mg^{2+} over Zn^{2+} in presence of TPEN both in intra- and exctracellular conditions.

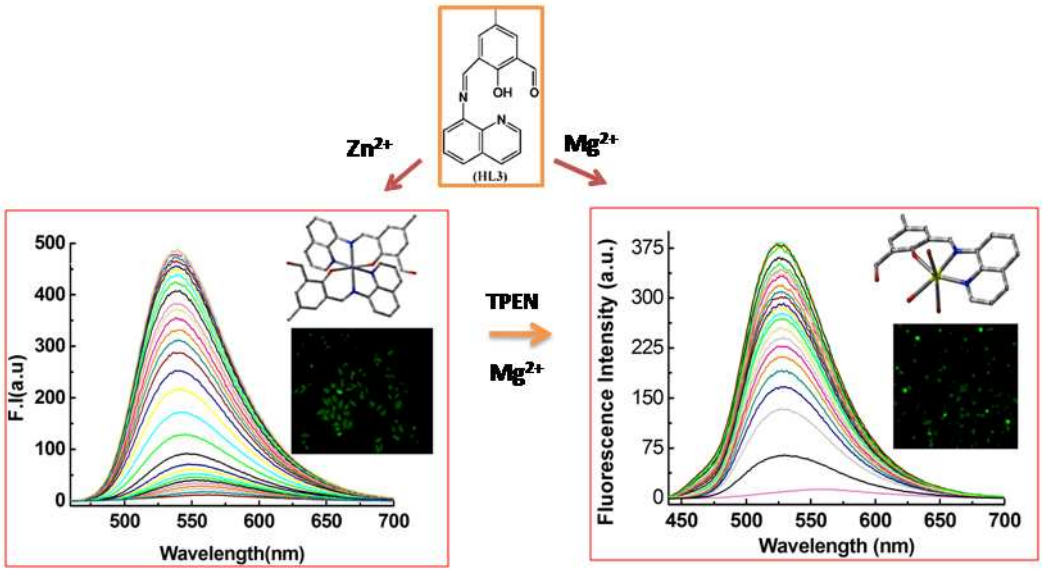

Cite this: DOI: 10.1039/c0xx00000x

www.rsc.org/xxxxxx

ARTICLE TYPE